Journal of Robotics and Control (JRC)
Volume 5, Issue 6, 2024
ISSN: 2715-5072, DOI: 10.18196/jrc.v5i6.22595

Active Vibration Isolation using Tilt Horizontal Coupling Immune Inertial Double Link Sensor for Low Frequency Applications

Vishnu G. Nair [1], Navya Thirumaleswar Hegde [2*], Dileep M. V. [3]
[1, 2] Dept. of Aeronautical and Automobile Engineering, Manipal Institute of Technology, Manipal Academy of Higher Education Manipal Udupi Karnataka, India 576104
[3] Dept. of Aerospace Engineering, Formerly with Chungnam National University, 99 Daehak-ro, Yuseong-gu, Daejeon, South Korea
Email: [1] vishnu.nair@manipal.edu, [2] navya.hegde@manipal.edu, [3] dileeppsla@gmail.com
*Corresponding Author

***Abstract*—Addressing the challenge of horizontal tilt coupling is crucial for using inertial sensors in precise applications, such as seismology and seismic isolation, including gravitational wave detection. Researchers have proposed various design solutions, with the Double Link (DL) sensor standing out for its sim- plicity, precision, and effectiveness. This paper explores the use of the DL sensor in an active vibration isolation system. We evaluated different control algorithms, including Proportional- Integral-Derivative (PID), Linear Quadratic Regulator (LQR), Linear Quadratic Gaussian (LQG), and H-infinity. Simulations conducted in the Simscape environment showed that the H-infinity controller performed best, achieving a significant reduction in vibration. While the current study is based on simulations, future work will focus on experimental validation to confirm the system's practical applicability and robustness in real-world scenarios. Our results demonstrate the potential of the DL sensor and LQG controller to enhance vibration isolation in low-frequency applications. Additionally, we conducted a detailed literature review on various methods used in similar applications. This review highlights alternative approaches, such as other sensor designs and control strategies, and discusses their advantages and limitations.**

Keywords—Double Link (DL) Sensor; Horizontal Tilt Coupling; Active Vibration Isolation; LQG Controller; Simscape Simulation; Inertial Sensors; Control Theory Applications; Low-Frequency Vi-Brations; Seismic Isolation; Gravitational Wave Detection.

I. INTRODUCTION

Has faced significant challenges, particularly in applications such as seismological studies and seismic isolation for gravitational wave detection. One major challenge is known as tilt horizontal (TH) coupling. This phenomenon occurs when inertial sensors, which are designed to measure movements, exhibit an unwanted interdependence between their horizontal and tilt axes. This interdependence can reduce the accuracy of the measurements, posing hurdles to achieving the desired precision in sensitive equipment. As the pursuit of accurate data collection becomes increasingly critical, overcoming such challenges becomes paramount. This paper addresses the intricacies of tilt horizontal coupling through the implementation of a double-link (DL) sensor—a solution that has garnered attention for its simplicity, precision, and efficiency. The foundational concepts and design strategies surrounding this sensor have been meticulously detailed in previous publications by the authors, setting the stage for the practical implementation explored in this work.

The objective of this study is to extend the theoretical advancements into real-world applications by integrating the double-link sensor into an active vibration isolation scenario. Seismic isolation applications, particularly in the realm of gravitational wave detection, demand not only precision but also resilience against external vibrations. Active vibration isolation is a technique used to reduce unwanted vibrations that can interfere with sensitive measurements, particularly at low frequencies where such disturbances are most challenging to mitigate. To address the challenges posed by tilt horizontal coupling, a comprehensive set of control algorithms has been employed. These include the widely used Proportional-Integral- Derivative (PID) controller, the Linear Quadratic Regulator (LQR), and the Linear Quadratic Gaussian (LQG) controller. Control algorithms are mathematical approaches used to regulate the behavior of systems, ensuring they perform as desired under various conditions. The rationale behind employing multiple algorithms is to evaluate and compare their efficacy in mitigating tilt horizontal coupling effects, providing a nuanced understanding of their performance under varying conditions.

Simulations constitute a vital aspect of this study, conducted within the Simscape environment—a virtual platform that allows for controlled testing and assessment of the system's efficiency and the robustness of the implemented algorithms. The results obtained from these simulations not only validate the theoretical advancements but also offer practical insights into the adaptability and effectiveness of the double-link sensor in real-world scenarios. By actively contributing to the ongoing advancements in gravitational wave detection technology, this research aligns with the broader mission of pushing the boundaries of precision instrumentation and paving the way for groundbreaking discoveries in the field of astrophysics. In summary, this paper represents a significant advancement in the understanding and application of the DL sensor introduced by the authors. By conducting a meticulous

analysis of its implementation, efficiency, and control mechanisms, the authors contribute valuable insights to the field of high-precision instrumentation, particularly in the context of seismic isolation and gravitational wave detection.

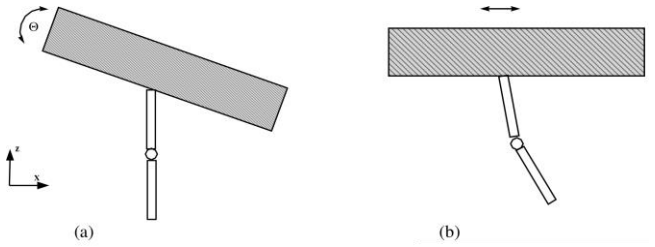

Fig. 1. Response of the double pendulum sensor to (a) Tilt and (b) Translation. The relative motion between the links are prominent in the case of translation and negligible during tilt [1]

Lows for controlled testing and assessment of the system's efficiency and the robustness of the implemented algorithms. The results obtained from these simulations not only validate the theoretical advancements but also offer practical insights into the adaptability and effectiveness of the double-link sensor in real-world scenarios. By actively contributing to the ongoing advancements in gravitational wave detection technology, this research aligns with the broader mission of pushing the boundaries of precision instrumentation and paving the way for groundbreaking discoveries in the field of astrophysics. In summary, this paper represents a significant advancement in the understanding and application of the DL sensor introduced by the authors. By conducting a meticulous analysis of its implementation, efficiency, and control mechanisms, the authors contribute valuable insights to the field of high-precision instrumentation, particularly in the context of seismic isolation and gravitational wave detection.

A. Double Link Sensor

This section introduces the sensor specifically engineered to effectively mitigate tilt horizontal (TH) coupling. The fundamental design of the sensor resembles a double pendulum system, comprising two links intricately connected to the platform through joints characterized by negligible stiffness. The envisioned scenario assumes a friction-less environment, ensuring the sensor's optimal functionality. The key output of the sensor is the relative motion between its two links. In essence, the sensor's responsiveness is finely tuned to the type of motion it encounters. During translational movements of the platform, the sensor generates a substantial output, providing a highly sensitive response. However, when the platform under- goes tilting motions, the output diminishes significantly. This unique characteristic stems from the negligible relative motion induced by tilting scenarios. The sensor's design, therefore, renders it exquisitely sensitive to translation while remaining nearly impervious to tilt effects (refer to Fig. 1 for a visual representation of the sensor).

This distinguishing feature positions the proposed sensor as a formidable solution for mitigating TH coupling, particularly at low frequencies. The sensor's innate insensitivity to tilt ensures that it effectively discriminates between horizontal translation and unwanted rotational influences. This selective sensitivity makes it a robust candidate for applications where precise translation measurements are paramount, such as in seismological studies and seismic isolation scenarios.

The determination of the Equations of Motion (EOM) for the proposed sensor system involves various methodologies, such as employing Newton's laws or the Lagrange method. The Lagrangian method is chosen for its effectiveness in capturing the dynamic behavior of the system. The equations of motion during translation and tilt is as follows. The reader is advised to refer [2] for an in-depth analysis on the sensor. For translation

$$\begin{gathered}\theta_1(s)(L_1M_1s^2 + L_1M_2s^2 - M_1s^2x_p(s) - \\ M_2s^2x_p(s) - L_2s^2 + s^2x_p(s) + k_1 + \\ \theta_2(s)\big(L_2M_2s^2\theta_2(s) - L_2s^2 + s^2x_p(s) + k_2\big) + \\ \theta_1(s)\theta_2(s)(L_2M_2s^2 - L_1s^2) = 0\end{gathered} \tag{1}$$

For tilt

$$\begin{gathered}\ddot{\theta}_d(1 - tan\theta_d) - \dot{\theta}_d\dot{\theta}_2 sin\theta_d + \dot{\theta}_1^2 sin\theta_d - \\ \frac{g}{L}sin\theta_2 - k_p\gamma - \frac{M_p gL}{2}sin\gamma = 0\end{gathered} \tag{2}$$

Fig. 2 illustrates the response of the proposed sensor concerning translation in the x-direction, and tilt about the y-axis. Notably, the sensor exhibits a high sensitivity to translation while demonstrating minimal sensitivity to tilt. These characteristic positions the sensor as highly efficient for various applications where mitigating tilt-horizontal (TH) coupling is imperative, such as in Gravitational Wave Detectors. Above the natural frequencies of the links, translation in the x-direction remains relatively constant at approximately -3.11 dB. Below these frequencies, the value progressively decreases. Additionally, tilt about the y-axis registers an order of magnitude approximately equal to 1010 below the reference point. This distinctive behavior signifies the efficacy of the proposed sensor in actively addressing TH coupling, showcasing its practical utility in scenarios demanding precise translation measurements while minimizing the impact of tilt-induced disturbances. Such performance attributes are particularly crucial in advanced applications like Gravitational Wave Detectors, where stringent precision requirements must be met. This paper focus on the implementation of the sensor in the low frequency active vibration isolation.

This paper makes several significant research contributions to the field of inertial sensor applications, particularly in addressing the challenges of horizontal tilt coupling in high- precision environments such as seismology and gravitational wave detection. Firstly, it introduces the Double Link (DL) sensor, demonstrating its effectiveness in active vibration isolation setups. The study also conducts a comparative analysis of various control algorithms, including PID, LQR, LQG, and H- infinity controllers, highlighting their respective strengths and weaknesses. Through frequency response analysis, the research provides insights into how these controllers can optimize system performance for low-frequency applications. Additionally, the paper offers valuable guidance on parameter tuning methodologies and implementation considerations, thereby enhancing the

practical utility of the proposed solutions. These contributions collectively advance the understanding of vibration control in critical scientific applications and lay a foundation for future research and real-world implementations.

The rest of the paper is organized as follows. Section 2 presents the recent developments in the field. The problem statement is discussed in section 3 followed by the implementation and control of the system for vibration isolation application in section 4. The results and discussions are given in section5 and section 7 concludes the paper with possible future research directions.

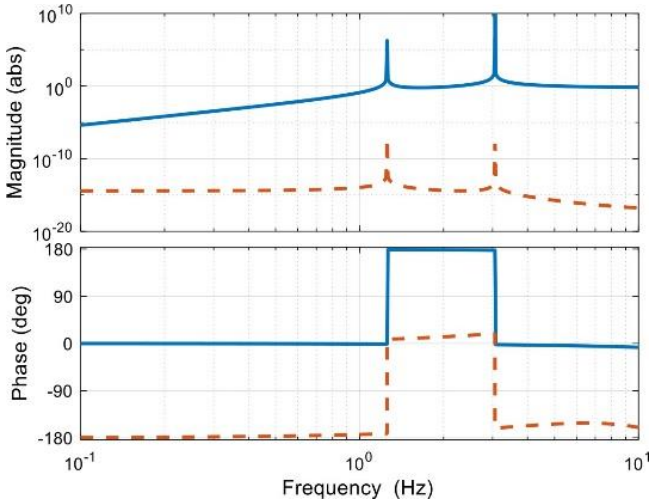

Fig. 2. The frequency response of the sensor to translation (blue line) and tilt (red line). The sensor is unresponsive to tilt motion as compared to translation [1]

II. DEVELOPMENTS TILL NOW

In addressing the challenge of tilt-horizontal (TH) coupling in the context of inertial sensors, various strategies have been explored and presented in the literature. An insightful review of TH coupling is given in [3], offering a comprehensive overview of methods proposed and implemented for its mitigation. Their analysis extends to the limitations associated with these approaches, emphasizing factors such as sensor noise and geometrical couplings. Collette, in [4], contributed to this discourse with an informative review on inertial sensors, delving briefly into the nuances of TH coupling.

Within the LIGO VIRGO collaboration, efforts to eliminate TH coupling involve two distinct approaches. The first explores the development of a seismometer designed to be insensitive to tilt within a specific frequency band [3; 5]. The second approach focuses on actively stabilizing the tilt motion of isolated platforms using 1D rotation sensors. Additionally, a patented scheme has been proposed to address TH coupling, wherein an absolute inertial sensor is affixed to the floor with a fixation rigid only in the tilting direction and compliant for the other degrees of freedom [6]. Hua, in his doctoral thesis [7], presented optimal Finite Impulse Response (FIR) complementary filters aimed at effectively separating tilt motion from horizontal acceleration. While these methods demonstrate efficacy, they often necessitate additional systems or structures, rendering them comparatively inferior to the sensor proposed in this paper. An alternative method proposed in the literature involves a novel approach referred to as '6D' [8]. This absolute inertial isolation scheme relies on a six degree-of-freedom (6D) interferometric readout of a single reference mass, demonstrating significant reduction in inertial motion at low frequencies. However, further investigation is required to evaluate its performance concerning TH coupling. In contrast, the double-link (DL) sensor proposed in this paper measures relative displacement/rotation between two suspended links, showcasing advantages in terms of simplicity and cost- effectiveness compared to other approaches. Various tilt and rotation measurement techniques have been explored, including beam-balances [9], tilt sensors composed of a bar suspended by a metallic glass flexure [10], and double-flexure two-axis tilt sensors with optical walk-off sensors [11]. These methods exhibit diverse sensitivities and applications, with some emphasizing high sensitivity to seismic noise. The challenges associated with existing approaches have led to continuous exploration of innovative solutions. The rotational vibration isolator presented by Sunderland *et al*. [12] in the form of a sphere plunged in a liquid showcases unique design features with an extremely low resonant frequency. Additionally, suspended seismometer models [13] and highly sensitive seismometers with an inverted pendulum and Michelson interferometer readout [14] have been proposed, each with its set of advantages and drawbacks.

In [15] a novel low-frequency active vibration isolation system, the compound pendulum, composed of two-dimensional elastic reeds and two pendulums is presented. In [16], enhancing the performance of ultra-stable lasers, particularly for non-laboratory and space applications is presented. Their work focuses on reducing the vibration sensitivity of the optical reference cavity, and through theoretical and experimental investigations on a 100 mm cubic cavity, they achieved a vibration sensitivity as low as 2×1011/g, paving the way for the development of a space-ready 1 Hz-linewidth laser system. Demir et.al [17], in their study, focuses on designing a horizontal vibration isolation system with adjustable quasi- zero-stiffness along three axes, achieved through a central string and tensioning mechanism. Parametric studies reveal that the system, capable of maintaining a broad isolation bandwidth from below 1 Hz to above 250 Hz, offers effective low- frequency vibration isolation. Chanh *et al*. [18] addresses the impact of micro-vibration on alkali-metal-noble-gas comagnetometers, crucial for fundamental physics and inertial navigation, by systematically analyzing their response to angular and linear vibration. Through experimental setup and optimization, including changes to structure, center of mass, and sensitive axis direction, the comagnetometer's vibration equivalent sensitivity is significantly reduced by approximately 20 times in the 1–4.75 Hz range. In [19], the authors presented a high-resolution Horizontal Interferometric Inertial Sensor (HINS) designed for gravitational wave detection instrument isolation, featuring a tunable resonance frequency of 0.08 Hz and achieving a resolution of 2×1013 m (or 7.9×1012 (m/s2)) at 1Hz through a Lehman pendulum, inverted pendulum mechanisms, and a novel homodyne quadrature interferometer. The dynamic analysis explores its response to diverse excitations, while a noise budgeting analysis reveals

limitations imposed by thermo- mechanical noise up to 1Hz and thermal electrical noise beyond 1Hz. In precision optical experiments, conventional pendulum systems often provide horizontal vibration isolation, but fail to address vertical vibrations. In [20], the authors introduced a novel pendulum actuator, utilizing a giant magneto strictive composite material, featuring a flexible wire made of a thin quartz fiber embedded in epoxy resin-bonded magneto strictive composite material with Terfenol-D particles, capable of isolating vertical vibrations. Experimental results demonstrate the actuator's linearity, with a sensitivity of 0.78 m/A to the driving current, an elongation range up to 5.9 m, and effective reduction of vertical environmental vibrations by 17.5 dB. Displacement sensors play a crucial role in gravitational wave detectors, with applications like the seismic isolation chain in LIGO utilizing optical shadow sensors for stabilization. The study conducted in [21] investigates the suitability of Birmingham Optical Sensors and Electromagnetic Motors (BOSEMs) for cryogenic applications through simulations and experimental tests, revealing their reliable operation at 100 K and improved performance, including a shot noise enhancement. In [22], the authors demonstrated the efficacy of combining ultra-low frequency vibration isolators with highly sensitive tilt sensing and feedback. The study showcases a reduction in rms vibration levels in laser interferometer gravitational wave detector test masses from 100 m to 1 nm. This approach claim to minimizes control system noise injection drastically.

In [23] The authors examines the application of a magneto- rheological (MR) damper in a semi-active isolator system, highlighting its ability to regulate damping force via an externally applied magnetic field and validating experimental results through the Viscous Plus Dahl Model. Integrating the MR damper with a fuzzy logic-based self-tuning PID controller in a marine diesel engine system, the study demonstrates significant improvements in vibration reduction compared to passive systems, particularly for a 1200 kg engine under various operating conditions. An experimental system for isolating low-frequency ground vibrations in cold atom interferometry combines passive vibration isolators with negative stiffness elements and a voice coil motor actuator, counteracting vibrations detected by a seismometer is developed in [24]. This setup, enhanced by a high- speed processor, reduces vertical vibration noise by a factor of 100 from 0.1 to 10 Hz, enabling precise gravity measurements with a cold atom gravimeter. The study in [25] introduces a new active negative stiffness (ANS) control strategy combined with sky-hook (SH) control to enhance low-frequency vibration isolation. Experimental validation shows that the ANS+SH strategy significantly reduces vibration transmissibility at the natural frequency from -1.45dB to -10.83dB, markedly improving low-frequency vibration control compared to SH control alone. In [26], the authors presents a novel noninteracting control strategy for a 6-degree-of-freedom (DoF) active vibration isolation system (AVIS) designed for high-precision machinery, addressing both external vibrations and internal interactions. The control law, incorporating state feedback, unity feedback, and feedforward from measured floor motion, ensures each DoF independently follows its reference, with robust stability achieved. In [27], the authors presents a maglev inertially stabilized platform (MISP) combining gimbals with magnetic bearings to eliminate low-frequency vibrations that mechanical isolation cannot address. An improved linear extended state observer (LESO) is proposed to enhance estimation accuracy by replacing displacement error with next-order error, and an active vibration isolation control method is designed to cancel the vibrations, with simulations validating the effectiveness of these measures in maintaining MISP stability. A hybrid bioinspired metamaterial with shape memory effect and programmable mechanical properties, designed using 4D printed shape memory polymer and bioinspired methods is presented in [28]. Compared to traditional nacre-like materials, these bioinspired metamaterials demonstrate enhanced adjustability in mechanical properties, impact resistance, and low-frequency vibration isolation, with experiments validating their performance and broad application prospects in impact protection and vibration absorption. The research in [29] examines a semi-active suspension damping control algorithm, proposing an improved particle swarm optimization strategy to address the limitations of traditional algorithms like the sky-hook and acceleration- driven damper algorithms. By utilizing a dynamic nonlinear inertia coefficient, the new algorithm optimizes nonlinear damping curves and, through simulations, demonstrates enhanced high-frequency vibration isolation, strong low-frequency resonance suppression, and improved vehicle driving comfort without significantly increasing spring mass jerk. Nonlinear quasi-zero-stiffness (QZS) vibration isolators are effective for vibration isolation but struggle with protecting masses that vary continuously. An adjustable absolute-zero-stiffness isolator that improves upon QZS isolators by incorporating sliding constraints with vertical side-springs and oblique cam-roller- spring units, achieving constant negative stiffness and validated through numerical simulations for various loads and seismic conditions is presented in [30]. In [31], the authors presented an active and passive vibration isolation system that enhances vertical vibration isolation for Raman mirror stability using linear bearings and voice coil motors, achieving a 98.34 pec reduction in vertical vibrations below 10 Hz and greatly improving the gravimeter's accuracy and reliability, with implications for both scientific research and industrial applications. Inspired by the Stewart platform, a theoretical model of a double- layered Stewart platform with local oscillators is proposed and studied in [32] through numerical simulations and experiments. Experimental results, validated using ADAMS software, show that the double-layered platform with oscillators effectively suppresses transmissibility near the resonant frequency, offering superior vibration isolation performance compared to traditional single-layered platforms.

Parallel mechanisms are used in high-precision vibration isolation systems but often exhibit unequal performance across different degrees of freedom (DOFs). An isotropic control framework that transforms a multi-DOF system into identical single-DOF systems, achieving uniform frequency response, corner frequency, active damping, and low-frequency transmissibility across all modes, demonstrated effectively with a 6-UPS parallel mechanism in [33]. To improve the vibration reduction and isolation performance of floating rafts for ship- borne equipment, a new approach

based on particle damping is proposed IN [34], addressing low-frequency vibration amplification issues. A mathematical model using gas-particle two- phase flow theory is developed and validated through dynamic analysis and experiments, demonstrating that particle damping significantly enhances the performance of floating rafts under low-frequency excitation, which is crucial for improving ships' operational effectiveness. In [35], the authors addresses the high demand for vibration isolation in micro/mini LED dis- play panel inspection by developing a self-stabilization device that combines passive and active strategies using piezoelectric ceramics (PZT) and voice coil motors (VCM). The device, optimized for lightweight design and controlled by a double compensating PID controller, achieved over 90 pec vibration isolation across 98 pec of the 1 to 500 Hz frequency range, significantly improved steady-state positioning accuracy, and effectively reduced VCM heat and disturbances, as validated through extensive testing. Increasing observation resolution in Earth observation satellites and space telescopes is hindered by vibrations from various sources, affecting the accuracy of space-borne precision optical payloads. To address this, a six-degree-of-freedom parallel strut isolation system using a Gough-Stewart configuration with flexible hinges is designed in [36], featuring a Fuzzy Auto-Disturbance Rejection Control strategy that demonstrates superior vibration isolation and robustness compared to traditional fuzzy PID control, as validated through dynamic analysis and simulations. A hybrid time-delayed feedforward and feedback controller (HTD-FFC) for lever-type QZS (L-QZS) isolators is introduced in [37], demonstrating through numerical and experimental analysis that HTD-FFC enhances vibration isolation performance, suppresses peak transmissibility, and eliminates instability, thereby im- proving overall robustness and stability. In [38], the authors introduced a compact, active vertical vibration isolator with a geometric ant spring (GAS) structure, significantly reducing measurement deviation in a homemade T-1 absolute gravimeter by a factor of 32, and is adaptable for different loads and suitable for both free-falling and atomic-interference absolute gravimeters. A very informative review on the developments of vibration isolation technologies in China is given in [39]. The study in [40] presented an analytical layer-element–boundary-element coupling approach to investigate the isolation effect of pile rows on moving-load induced vibrations in stratified transverse isotropic saturated media. Numerical examples reveal that while stiffer piles significantly enhance vibration reduction, increasing pile length beyond a certain point does not improve isolation, and the material anisotropy of the soil also plays a crucial role. A novel magnetic-suspended (MS) geophone is developed to improve low-frequency performance by using four concentric magnetic cylinders as a magnetic spring to suspend the proof-mass, with two compensating coils driven by adjustable currents to maintain low linear stiffness and compensate for magnetic force errors in [41]. The prototype, exhibiting a natural frequency of 0.59 Hz and a sensitivity of 412 V/(m/s), demonstrates effective low-frequency performance with a proof-mass excursion within ±1.2 mm, making it suitable for low-frequency active vibration isolation applications. Most seismic isolation devices only address horizontal ground acceleration, but [42] introduced a novel inertia-type bidirectional isolation system (IBIS) that isolates both vertical and horizontal ground motion. The IBIS, featuring a vertical isolator with a leverage apparatus and a conventional sliding-type horizontal isolator, demonstrates high isolation performance and anti- resonance properties under both near-fault and far-field ground acceleration, with the vertical isolator effectively balancing the isolated object's self-weight and enhancing dynamic stability.

To meet stringent ultra-low frequency vibration isolation requirements for high-precision equipment, an active vibration isolation method using electromagnetic suspension is investigated in [43]. Theoretical and experimental results demonstrate that this method effectively improves vibration isolation performance, maintaining transmissibility below 0 dB across the entire frequency band and achieving an initial isolation frequency of less than 1 Hz. In [44], the authors introduced an active-passive integrated vibration isolator using piezoelectric ceramics, designed to enhance the positioning and control accuracy of high-precision equipment by mitigating low-frequency vibrations. The isolator combines a piezoelectric actuator and a damping buffer, effectively attenuating vibrations from 5 Hz to 500 Hz, with experimental results showing up to 30 pec reduction in excitation amplitude, thereby broadening the applicable frequency range for industries like aerospace and precision equipment manufacturing. A novel truss-spring structure enhanced by an inertial mechanism (TCTS-RIM), inspired by triangulated cylindrical origami, to address the challenge of low-frequency vibration isolation with tunable stiffness and inertia is presented in [45]. The system utilizes a modified crease simulation mechanism to achieve a quasi-zero stiffness (QZS) range, enhancing the engineering feasibility and dynamic performance of volumetric origami structures, as demonstrated by both theoretical analyses and experimental validation. A novel three-axis levelling and active-passive vibration isolation (LAPV) composite stage, designed to achieve micro-meter- level precision in chip alignment for white-light-interference topography by combining a modified quasi-zero-stiffness mechanism with voice coil motors for active control is studied in [46]. The stage achieves precise levelling with a deviation of only 33.2 rad and effectively isolates vibrations across a broad frequency range, demonstrating up to 90 pec isolation effectiveness through experimental validation. An active geophone using a magnetic spring (AG-MS), where a reference mass is suspended by a frictionless, three-layer magnetic spring system, enhancing low-frequency measurement capabilities by using two winding coils to shape magnetic force, ensure linearity, and maintain low stiffness is presented in [47]. The prototype of the AG-MS demonstrated improved performance with a measurement bandwidth of 0.1 Hz to 28 Hz and a sensitivity of 158 V/(m/s), significantly reducing the nonlinearity issues typical of traditional geophones. To address high vibration levels in high-speed train floors, a study [48] implemented multiple dynamic vibration absorbers (DVAs), analyzing the causes through operational and modal tests, and modeling the vehicle body with DVAs based on the modal superposition method. The research successfully attenuated dominant low- frequency vibrations using a single under-frame DVA and controlled

multiple local modes between 30 and 35 Hz with optimized multiple DVAs, significantly enhancing ride quality by reducing vertical motion. A coarse and fine parallel vibration isolation pointing platform (CFPP) designed for space optical payloads has been developed, utilizing a Stewart generalized configuration for a wide range of motion and effective active vibration isolation [49]. Through extensive testing, including a three-axis pointing range and active vibration isolation experiments across four attitudes, the platform demonstrated a movement range of 7 degrees on three axes and achieved up to 20 dB vibration isolation in the 2-20 Hz frequency band, showcasing significant potential for future applications. An enhanced adaptive feedforward vibration isolation technique that utilizes a weighted transformation matrix derived from singular value decomposition to effectively mitigate slow convergence and stability issues inherent in classical FxLMS algorithms is introduced in [50]. Validated through multi-axis system simulations, this method demonstrated up to 70 dB attenuation in the 0.1 to 100 Hz frequency range and maintained a relative parameter error below 6 pec, suggesting its applicability in the active vibration isolation of space telescopes and precision optical instruments. A novel passive structure inspired by the postures of a click beetle, termed CBIS (Click-Beetle-Inspired Structure), featuring variable asymmetric stiffness, has been developed in [51] to facilitate stiffness tuning and enhance low-frequency vibration isolation. Utilizing three rods and two springs, the CBIS can adjust its stiffness across a spectrum from negative to small positive, including zero and quasi-zero stiffness states, significantly broadening its effective range and lowering the resonant frequency to under 2 Hz for superior vibration isolation performance. A compression-twist coupled metamaterial inspired by Kresling origami, designed to provide strong force support and optimal structural design within limited space, particularly for aerospace applications is presented in [52]. Through detailed investigation of its vibrational response and bandgap characteristics, along with parametric studies and experimental validation, the research offers valuable insights into the dynamics control and bandgap tuning of origami- inspired metamaterial structures.

A novel low-stiffness gear with replaceable blades designed to effectively isolate micro-vibrations in high-precision space payloads such as antennas is presented in [53]. Using the second-order deformation theory of cantilever beams, the study established a nonlinear transmission stiffness model and validated its vibration isolation performance through static and ground equivalent tests, demonstrating its reliability for use in the Solar Array Drive Assembly. The progress of quasi- zero-stiffness (QZS) vibration isolation technology, highlighting its superior performance in low-frequency isolation compared to traditional methods, and summarizes the latest designs, improvement strategies, and applications is reviewed in [54]. Microgravity vibration isolation control within a space station by using an actor-critic neural network to estimate combined disturbances and develop compensatory strategies, alongside an adaptive robust term to manage estimation errors is investigated in [55]. Simulations demonstrate that the proposed controller effectively stabilizes the system and significantly suppresses onboard vibration amplitudes by approximately 60 dB in the 2 to 100 Hz frequency range. A tunable local resonance metamaterial with chiral buckling structures designed for low-frequency vibration isolation is introduced in [56]. The study shows that unit cells with initially convex downward beams exhibit strong bistability and significantly different axial stiffness in their stable states, while hybrid supercells further enhance band gap width and lower the band gap frequency, offering up to 16 distinct band gap characteristics.

An adjustable anti-resonance frequency controller for a dual- stage actuation semi-active vibration isolation system (DSA- SAVIS) designed to mitigate inertial force disturbances during frequency sweeping in semiconductor manufacturing is presented in [57]. Experimental results demonstrate that this system significantly reduces vibration amplitude, achieving closed-loop transmissibility below 15 dB up to the initial anti- resonance frequency and below 30 dB around an adjustable anti-resonance frequency, leading to an 87.5 pec reduction in disturbance amplitude. A frequency-adjustable dynamic vibration absorber (DVA) with a single degree-of-freedom (DOF) quasi-zero-stiffness (QZS) vibration isolator to enhance vibration isolation performance is presented in [58]. The coupled system reduces the initial vibration isolation frequency, broadens the effective vibration reduction bandwidth, and im- proves low-frequency isolation by adjusting key parameters and leveraging anti-resonance characteristics. The study in [59] introduces the ABVS-EMVI, a novel bionic vibration isolation device that combines an active bionic variable-stiffness device with an electromagnetic system to improve vibration isolation and enable energy harvesting. Dynamic equations for the spacecraft-adapter system with ABVS-EMVI are derived, and results show that the electromagnetic system enhances both vibration isolation performance and energy harvesting capabilities under various excitation conditions. A novel bionic quasi-zero-stiffness (QZS) vibration isolator inspired by the human spine, featuring a cascaded multi-stage negative stiffness structure to address low-frequency vibrations (2-5 Hz) more effectively than traditional isolators is presented in [60]. Numerical analysis reveals that increasing the number of negative stiffness stages and reducing damping and external force values significantly enhance low-frequency isolation performance, outperforming linear structures and existing QZS isolators. The review in [61] explored the advancements in nonlinear vibration isolation technology over the past twenty years, focusing on the quasi-zero-stiffness (QZS) vibration isolators, particularly the “three-spring” configuration, which offers superior low- frequency isolation by exploiting beneficial nonlinearities. Emphasizing the fast response, strong stroke, and cost-effectiveness of electromagnetic mechanisms, the review discusses the basic theory, design methodology, nonlinear damping mechanisms, and active control of electromagnetic QZS isolators, and pro- vides future research perspectives for enhancing vibration isolation efficiency. A bilateral supported bio-inspired anti-vibration (BBAV) structure, designed with purely linear elements and inspired by bird leg motion and muscle-tendon dynamics, to improve low-frequency vibration isolation is introduced in [62]. Analysis reveals that by adjusting key parameters such as spring stiffness, rod length, and installation angle, the BBAV structure achieves superior vibration isolation

performance and can switch between softening and hardening nonlinear behaviors, offering a tunable and effective anti-vibration solution.

In [63], the authors proposed a quasi-zero stiffness (QZS) isolator inspired by the precise capturing ability of spiders in vibrating environments, composed of a curved beam and a linear spring, which can significantly reduce the first-order natural frequency under load. Their harmonic balance method (HBM) analysis, verified by the fourth-order Runge-Kutta method (RK-4), showed the isolator's lower initial isolation frequency and wider bandwidth compared to equivalent linear isolators. Similarly, in [64], an active adjustable high-static- low-dynamic-stiffness (HSLDS) vibration isolator using pro- portion integration (PI) controllers and piezoelectric actuators was introduced, which effectively reduced resonant amplitude and broadened isolation frequency bandwidth. Meanwhile, [65] studied the vibration isolation effect of double-layer wave impeding blocks (WIB) in unsaturated ground, revealing that designing the wave impedance ratio at the layer intersection improved isolation effectiveness, especially at lower soil saturation levels. Furthermore, [66] designed a novel three- degree-of-freedom (3-DOF) passive vibration isolation unit with enhanced QZS effect and beneficial nonlinear stiffness and damping properties, achieving superior ultra-low-frequency vibration isolation in three directions. [67] proposed an active bionic variable stiffness adapter (ABVSA) inspired by ostrich motion for spacecraft payloads, demonstrating its effectiveness in reducing vibrations during launches through a PID-controlled system, validated by numerical results and nonlinear output frequency response functions (NOFRFs). In [68], an X-shaped structure was integrated into a two-stage vibration isolation system to achieve broadband isolation, with its nonlinear equation of motion derived using the Lagrange equation and validated through simulation and experiments. The system's frequency response and isolation performance, particularly in the 2-5 Hz range, were significantly improved by softening nonlinearity. Inspired by kangaroo legs, [69] introduced a bio-inspired kangaroo leg structure (BKLS) for low-frequency vibration isolation, demonstrating high-static and low-dynamic stiffness (HSLDS) properties over a wide displacement range and effective sup- pression of vibrations above 1.06 Hz. Similarly, [70] presented a bio-inspired vibration isolation–absorption (BIVIA) system inspired by ostrich anatomy, achieving wideband isolation and high stability through a toe-leg-spine coupling structure. The system's QZS characteristics and performance were optimized by designing key parameters. In [71], a novel QZS isolator using a disc spring group and volute spring was proposed, offering an extended QZS range and large loading capacity by compensating nonlinear stiffnesses. This design outperformed traditional QZS and X-shaped structures in vibration isolation under heavy loads. [72] explored multistage oscillators for ultra-low frequency vibration isolation and energy harvesting (VIEH), combining mechanical coupling and electromechanical conversion technologies to reduce initial frequencies and maximize output power, validated by experimental results.

Extensive research has significantly improved the vibration isolation performance of off-road vehicle seat suspensions, addressing issues such as driver fatigue and low-back pain. However, variations in road roughness, vehicle speed, and load can lead to instability and sudden events in seat vibration excitation. To address this, [73] proposed an intelligent damping switching method using a long short-term memory (LSTM) network and multi-input multi-output optimization (MIMO) method, effectively maintaining suspension deflection and im- proving vibration isolation. In [74], a new vibration isolator with a wide range of zero-stiffness was developed, combining three negative stiffness mechanisms for superior performance over traditional QZS and linear isolators. Meanwhile, [75] introduced a genetic algorithm-back propagation neural network PID control (GA-BP-PID) for active vibration-isolation systems (AVIS) in ultra-precision machining, demonstrating improved efficiency under dynamic load conditions. Similarly, [76] designed a novel vehicle-mounted QZS vibration isolator with an H-infinity optimal control strategy, showing excellent isolation effects for both large and small amplitude excitations. Additionally, the Fluid Physics Research Rack (FPR) on the Chinese Space Station employs the Microgravity Active Vibration Isolation System (MAVIS), which uses electromagnetic actuators and high-precision sensors to achieve a microgravity level of 1-30 g0 in the frequency range of 0.01-125 Hz, as demonstrated by in-orbit tests, providing a stable environment for microgravity experiments [77]. Extensive research has led to various advanced vibration isolation systems to enhance performance in different applications. For microsatellites, a six-degree-of-freedom (6-DOF) vibration isolation platform with MnCu alloy helical springs effectively reduces micro- vibrations, achieving a minimum initial isolation frequency of 16.8 Hz and a suppression effect of up to 17.5 dB [78]. Vehicle vibration isolation performance under low-frequency excitation is improved by simultaneously adjusting stiffness and damping through an acceleration-driven-stiffness fuzzy control strategy (ADSFC) and Skyhook-based fuzzy control strategy (SHFC), significantly outperforming passive suspensions [79]. In tunnel boring machines (TBM), a single-degree-of-freedom active isolation system driven by a voice coil motor, utilizing a hybrid control strategy optimized by a genetic algorithm, achieves displacement attenuation of less than -17 dB and acceleration attenuation of less than -21 dB [80]. A dual four-rod horizontal vibration isolator for medical precision instruments, optimized with an artificial fish swarm algorithm, exhibits excellent low-frequency vibration isolation, showing lower initial isolation frequency and wider bandwidth [81]. Lastly, Glass Fiber Reinforced Composite (GFRC) materials integrated into a mechatronic control system for industrial machinery significantly reduce transmitted vibrations, achieving reductions of 98.46 pec and 98.5pec for different GFRC configurations [?].

In conclusion, while each method contributes valuable insights and solutions to the TH coupling challenge, there remains a need for comprehensive evaluations considering factors such as complexity, cost-effectiveness, and performance in handling coupling. This paper offers a promising alternative with potential advantages over existing methods. The continuous exploration and refinement of such

techniques underscore the dynamic and evolving nature of the field of low-frequency vibration isolation.

III. PROBLEM STATEMENT

The field of high-precision instrumentation, particularly in applications like seismological studies and seismic isolation for gravitational wave detection, faces a significant challenge known as tilt horizontal coupling. This phenomenon, characterized by interdependence between the horizontal and tilt axes of inertial sensors, poses substantial obstacles to achieving desired levels of precision in sensitive equipment. Overcoming these challenges is crucial as accurate data collection becomes increasingly vital, particularly in specialized fields like gravitational wave detection. Various design strategies have been proposed by researchers to address tilt horizontal coupling, among which the double-link sensor stands out due to its simplicity, precision, and efficiency. Previous publications have thoroughly documented the foundational concepts and design strategies behind this sensor, providing a theoretical basis for its practical implementation. The objective of this study is to bridge the gap between theoretical advancements and real-world applications by integrating the double-link sensor into an active vibration isolation scenario. In seismic isolation applications, especially for gravitational wave detection, precision and resilience against external vibrations are paramount. Low- frequency active vibration isolation is particularly crucial in enhancing sensitivity and reliability in these specialized fields. To address the challenges posed by tilt horizontal coupling, this study employs a comprehensive set of control algorithms, including PID, LQR, LQG and H-infinity controllers. The rationale behind using multiple algorithms is to assess and compare their efficacy in mitigating tilt horizontal coupling effects under varying conditions. Simulations conducted within the Simscape environment serve as a controlled testing ground to evaluate the system's efficiency and the robustness of the implemented algorithms. This research aims to provide practical insights into the adaptability and effectiveness of the double- link sensor in real-world scenarios, thereby advancing the field of high-precision instrumentation and seismic isolation.

IV. IMPLEMENTATION AND CONTROL

This section provides an overview of the implementation of the DL (double-link) sensor and the design of controllers within the system. Initially, the setup is described, detailing the arrangement of components. Subsequently, the implementation of various controllers, including PID, LQG, LQR, and H- infinity controllers, is discussed.

A. Practical Implementation of the System

This section provides an overview of the practical application of the DL (double-link) sensor in a real-world scenario, illustrated in Fig. 3. In this setup, vibrating forces acting on the ground are transmitted to a table, which is our subject of interest. The objective is to implement an active vibration control system that renders the table insensitive to ground vibrations. The DL sensor is mounted underneath the table, as depicted in the Fig. 3. Although the sensor's size is shown as comparable to the table for illustrative purposes, it is typically much smaller in reality. The primary focus here is on the horizontal translation and tilt motion of the table. Although the table may experience six degrees of freedom motion due to ground vibrations, our emphasis is on showcasing the efficiency and implementation of the DL sensor in such scenarios. It's important to note that a future direction of this research involves developing a six- degree-of-freedom DL sensor. The vibrations sensed by the DL sensor are relayed to the controller, which then generates appropriate control signals to actuate the horizontal and vertical actuators placed on the table. This process effectively achieves vibration isolation and enhances the stability of the table.

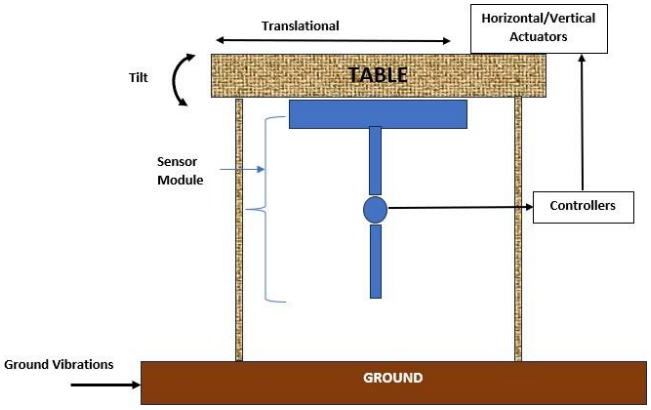

Fig. 3. Practical implementation of proposed sensor system. The DL (double- link) sensor, shown here for visualization purposes, is positioned beneath the table to monitor and counteract vibrations. Note that while the sensor's size is depicted comparably to the table for clarity, it is typically significantly smaller in real-world applications

B. Controller Design

As illustrated in Fig. 3, the controller constitutes the central component of the vibration isolation system. Given that this paper focuses on vibration isolation at low frequencies for high-precision instruments like gravitational wave detectors, a thorough comprehension of the control methodology is crucial. The primary aim is to keep the system as straightforward as possible. Several control algorithms are implemented in the system, including PID and its variants, LQR, LQG, H-infinity, and MPC. The objective is to assess the performance of each algorithm within the proposed system and draw comparisons between them. This analysis will serve to guide future practical implementations. A brief description on each of these controllers is given in following sections.

1) PID Controller and its Variants:

The Proportional (P) controller is a fundamental component in control systems, providing a response to the error between the desired setpoint and the actual process variable. Its simplicity lies in its direct proportionality between the error and the control signal it generates. By multiplying the error by a proportional gain Kp, the controller adjusts the system in proportion to the magnitude of the error. For readers unfamiliar with PID control, we recommend the foundational text "Feedback Control of Dynamic Systems" [82] by Gene Franklin, J. David Powell, and Abbas Emami-Naeini for a comprehensive introduction. While the P controller can effectively eliminate steady-state error, it may

introduce oscillations or instability if used in isolation, especially in systems with significant dynamic behavior or disturbances. Expanding upon the P controller, the Proportional-Integral (PI) controller introduces an integral term to address steady-state error. By accumulating the error over time and integrating it, the PI controller ensures that the system settles precisely at the desired setpoint, eliminating any residual error. This integral action, in conjunction with the proportional response, provides stable and accurate control, making the PI controller suitable for systems with unknown or variable disturbances. Incorporating a derivative term, the Proportional-Derivative (PD) controller enhances the response of the control system by predicting the future trend of the error. The derivative action dampens the response, reducing overshoot and oscillations. While the PD controller improves response time and stability compared to the PI controller, it may be sensitive to noise or high-frequency disturbances. Thus, proper tuning is crucial to balance the proportional, integral, and derivative actions for optimal performance.

Combining all three terms, the Proportional-Integral-Derivative (PID) controller offers a comprehensive solution to control challenges. The overall control function of a PID (Proportional-Integral-Derivative) controller is represented by the equation: control input 'u' w.r.t. the reference input is given by

$$u(t) = K_p e(t) + K_i \int e(t)dt + K_d \frac{d}{dt} e(t) \quad (3)$$

Where error can be formulated as in (4)

$$e(t) = s_p - p_v(t) \quad (4)$$

Here '$p_V(t)$' is the control variable at instantaneous time at 's_P', is the reference position. By balancing response speed, stability, and steady-state accuracy, the PID controller is versatile and widely used across various industries and applications. However, tuning the three parameters (Kp, Ki, Kd) can be complex, requiring careful consideration of system dynamics and performance requirements.

Parameter Tuning Methodologies: The tuning of PID parameters is critical to achieving optimal performance. In this study, the Ziegler-Nichols method was primarily used, which involves setting the integral and derivative gains to zero, increasing the proportional gain until the system reaches the ultimate gain, and then using this value to set the integral and derivative gains based on predefined formulas. Additionally, other heuristic approaches, such as trial and error and manual fine-tuning, can be employed to refine the parameters further. These methods help ensure that the PID controller responds effectively to various disturbances, providing a balance between responsiveness and stability.

Stability Analysis Criteria: To ensure the stability of the PID-controlled system, root locus and Bode plot analyses are generally conducted. The root locus analysis involves plotting the possible locations of the closed-loop poles as the proportional gain varies, ensuring that all poles remain within the left half of the complex plane, which indicates a stable system. Bode plot analysis, on the other hand, provides a frequency-domain view, showing the gain and phase margins that contribute to system stability. By verifying that these margins are adequate, we can ensure that the system will not oscillate or become unstable under normal operating conditions.

Implementation Considerations: The practical implementation of the PID controller can be carried out using a digital signal processor (DSP), which was integrated with the Double Link (DL) sensor. The DSP allows for high-speed computation of the control algorithms and real-time processing of sensor data. The DL sensor, mounted underneath the table, provides real-time feedback on horizontal translations and tilt motions. This feedback is crucial for the PID controller to adjust the control signals accurately and promptly. The DSP processes the sensor data, computes the required control actions, and sends signals to the actuators to mitigate vibrations. This setup ensures that the table remains stable and insensitive to ground vibrations, demonstrating the effectiveness of the PID controller in an active vibration isolation system.

2) LQR Controller:

The Linear Quadratic Regulator (LQR) controller stands as a cornerstone in control theory, offering optimal solutions for linear time-invariant (LTI) systems. At its core, the LQR controller aims to minimize a quadratic cost function over an infinite time horizon, leveraging state feedback to achieve this goal. This quadratic cost function typically takes the form:

$$J = \int_0^\infty (x^T Q x + U^T R u) dt$$

Here, *J* represents the total cost, x denotes the state vector of the system, and u symbolizes the control input. The matrices *Q* and *R* act as weighting matrices for the state variables and control inputs, respectively.

The control law prescribed by the LQR controller is elegantly simple:

$$u(t) = -Kx(t)$$

Where K represents the state feedback gain matrix. The optimal state feedback gain matrix K is determined by solving the associated Algebraic Riccati Equation (ARE), a differential equation known for its central role in LQR control. The solution to the ARE furnishes the optimal gain matrix that minimizes the specified cost function, thereby facilitating optimal closed-loop control. A good starting point for understanding LQR control is "Optimal Control Theory: An Introduction" by Donald E. Kirk [83].

LQR controllers are esteemed for several key properties. Firstly, they offer optimal control solutions, striving to minimize the specified cost function over an infinite time horizon, subject to the system dynamics and control constraints. Additionally, LQR controllers exhibit robustness to disturbances and un- certainties, owing to their inherent feedback from the system state. Moreover, stability of the closed-loop system is ensured provided the system is

stabilizable and detectable, allowing for effective state observation and control. Practical implementation of LQR controllers warrants careful consideration. Tuning of the weighting matrices Q and R is paramount, as it directly influences the performance of the controller. Efficient numerical algorithms are employed to address the computational complexity associated with solving the Riccati equation, especially for large-scale systems. Furthermore, LQR control necessitates full- state feedback, implying that all state variables of the system must be measurable or estimable.

Parameter Tuning Methodologies**:** The tuning of the LQR controller involves selecting appropriate weights for the cost function, which are typically represented in the quadratic cost function as matrices Q and R. These weights determine the relative importance of the state variables and control inputs. The selection process is based on performance requirements and system dynamics. Initially, a set of weights can be chosen through trial and error, adjusting the values based on the system's response to disturbances. Optimization techniques, such as genetic algorithms or gradient descent, can also be employed to fine-tune the weights for optimal performance. This iterative process helps in achieving a balanced trade-off between control effort and system stability, ensuring that the system performs optimally under various conditions.

Stability Analysis Criteria: The stability of the LQR-controlled system is guaranteed by the properties of the Riccati equation, which is a fundamental part of the LQR design. The Riccati equation is solved to obtain the optimal gain matrix K. For the system to be stable, the solution of the Riccati equation must yield a positive definite matrix. This positive definiteness ensures that the closed-loop system is stable and that all state variables will converge to their desired values over time. The eigenvalues of the closed-loop system matrix (ABK) should lie in the left half of the complex plane, confirming the stability of the system. This rigorous mathematical foundation provides a robust framework for ensuring the stability of the LQR controller.

Implementation Considerations: The practical implementation of the LQR controller involves several steps. First, the Riccati equation is solved offline, which involves calculating the optimal feedback gain matrix K based on the selected Q and R weights. This offline computation ensures that the LQR controller is computationally efficient during real-time operation. The resulting feedback gains are then programmed into the controller. The LQR algorithm is generally executed on a real-time operating system (RTOS), which provides the necessary computational power and timing accuracy for timely control actions. The RTOS ensures that the control signals are computed and applied to the actuators with minimal delay, maintaining the system's responsiveness to disturbances. The integration of the LQR controller with the RTOS and the Double Link (DL) sensor system provides a robust solution for active vibration isolation, demonstrating its effectiveness in maintaining the stability and precision of the controlled system.

3) LQG Controller:

Linear Quadratic Gaussian (LQG) com- bines Linear Quadratic Regulator (LQR) control and Kalman filtering. As already explained in the previous section, the LQR control aims to design optimal state feedback controllers for linear systems, optimizing a cost function that balances system performance against control effort. Meanwhile, the Kalman filter, an optimal state estimator, processes noisy sensor measurements to iteratively refine the system state estimate, accounting for both system dynamics and measurement uncertainties through prediction and update steps.

Prediction Step:

$$\hat{x}_{k|k-1} = A\hat{x}_{k|k-1} + Bu_{k-1}$$

$$P_{k|k-1} = AP_{k-1|k-1}A^T + Q$$

Where, $\hat{x}_{k|k-1}$ is the predicted state estimate at time k given measurements up to time $k - 1$. $P_{k|k-1}$ is the predicted error covariance matrix at time k given measurements up to time $k - 1$. Q is the process noise covariance matrix.

Update Step:

$$K_k = P_{k|k-1}C^T(CP_{k|k-1}C^T + R)^{-1}$$

$$\hat{x}_{k|k} = \hat{x}_{k|k-1} + K_k(yk - C\hat{x}_{k|k-1})$$

$$P_{k|k} = (I - K_kC)P_{k|k-1}$$

Where, K_k is the Kalman gain at time k. R is the measurement noise covariance matrix. y_k is the measured output at time k. I is the identity matrix.

The fusion of LQR and Kalman filtering forms the basis of LQG control, offering a robust and optimal control framework capable of managing uncertainties and disturbances. In an LQG control system, the Kalman filter estimates the system state based on noisy measurements, while the LQR controller computes the optimal control input based on this estimated state. This synergy empowers the controller to make informed decisions amidst noisy environments, calculating the accurate state estimation from the Kalman filter to optimize control inputs, ultimately minimizing the expected cost function value. For an in-depth exploration of LQG control, "Linear Systems Theory" by Joao P. Hespanha is a highly recommended resource [84].

Parameter Tuning Methodologies: Tuning the LQG controller involves adjusting the parameters of the Kalman filter, which estimates the system states based on noisy sensor measurements. The Kalman filter parameters are typically represented by the process noise covariance matrix Q and the measurement noise covariance matrix R. These parameters are tuned to minimize the estimation error, ensuring accurate state estimation. Methods such as the innovation sequence and auto correlation methods are employed for this purpose. The innovation sequence involves analyzing the difference between the predicted and actual measurements, adjusting the parameters to minimize this difference. The auto correlation method examines the correlation of the estimation errors over

time, tuning the parameters to reduce these correlations. These methodologies help achieve optimal performance of the Kalman filter, leading to accurate state estimates that enhance the overall effectiveness of the LQG controller.

Stability Analysis Criteria: The stability of the LQG-controlled system is analyzed by ensuring that the combined system of the controller and estimator meets the separation principle. The separation principle states that the design of the state estimator (Kalman filter) and the design of the state feedback controller (LQR) can be carried out independently. The stability of the combined LQG system is guaranteed if both the Kalman filter and the LQR controller are stable individually. This principle simplifies the design process and ensures that the overall system remains stable. Specifically, the eigenvalues of the closed-loop system matrix (formed by combining the controller and estimator gains) should lie in the left half of the complex plane. This condition ensures that the system will not exhibit oscillatory or divergent behavior, maintaining stable operation under varying conditions.

Implementation Considerations: The practical implementation of the LQG controller involves executing state estimation and control law computation in parallel to ensure real-time performance. The Kalman filter continuously estimates the current states of the system based on noisy measurements, providing these estimates to the LQR controller. The LQR controller then computes the optimal control actions based on the estimated states. This parallel execution is typically man- aged by a real-time operating system (RTOS), which ensures that both estimation and control processes are performed with minimal delay. The integration of the LQG controller with the Double Link (DL) sensor system involves setting up the Kalman filter to receive real-time feedback from the sensors, processing this data to estimate the states accurately. The estimated states are then used by the LQR controller to generate control signals that actuate the system, mitigating vibrations and enhancing stability. This implementation ensures that the LQG controller operates effectively in real-time, maintaining system performance even in the presence of measurement noise and uncertainties.

4) H-infinity Controller:

A H-infinity controller is a robust control strategy used to design controllers for dynamic systems that are subject to uncertainties and disturbances. Unlike traditional control techniques, which often aim to minimize the effect of disturbances in a certain frequency range or ensure stability under specific conditions, H-infinity control seeks to minimize the worst-case effect of disturbances across all frequencies. This makes H-infinity control particularly well-suited for systems with uncertain or time-varying dynamics. To apply H-infinity control, the dynamic system is typically represented in state-space form as

$$\dot{x}(t) = Ax(t) + Bu(t) + Ew(t)$$

$$y(t) = Cx(t) + Du(t) + Fw(t)$$

Where, $x(t)$ represents the state vector of the system. $u(t)$ represents the control input. $y(t)$ represents the output. $w(t)$ represents the disturbance input. *A*, *B*, *C*, *D*, *E*, and *F* are matrices representing the system dynamics.

The key idea behind H-infinity control is to minimize the H_∞ norm of the transfer function from disturbances to controlled outputs, subject to performance and stability constraints. The H_∞ norm represents the maximum amplification of disturbances to the controlled outputs across all frequencies. The optimization problem can be formulated as finding a controller *K* that minimizes the H_∞ norm of the closed-loop transfer function $T(s)$:

$$\min_K \|T(jw)\|_\infty$$

One of the key advantages of H-infinity control is its ability to provide robust stability and performance guarantees in the presence of uncertainties and disturbances. By minimizing the worst-case effect of disturbances, H-infinity controllers can ensure stable and reliable operation even in challenging operating conditions. However, there is often a trade-off between robustness and performance. Designing controllers to be more robust to uncertainties may result in degraded performance in terms of tracking accuracy or control effort. Balancing these trade-offs typically involves tuning controller parameters and selecting appropriate weighting functions in the optimization problem. To get an in depth understanding of H-infinity control, "Robust and Optimal Control" by Kemin Zhou, John C. Doyle, and Keith Glover provides an excellent foundation [85].

Parameter Tuning Methodologies: Tuning the H-infinity controller involves solving the H-infinity optimization problem, which is typically done using numerical algorithms. These algorithms aim to find the controller that minimizes the H- infinity norm of the closed-loop transfer function, representing the worst-case gain from disturbances to the system output. The process begins with formulating the control problem in terms of a state-space model, including the performance and robustness requirements. Numerical optimization techniques, such as the Riccati-based approach or linear matrix inequalities (LMIs), are then used to solve the H-infinity problem. These methods iteratively adjust the controller parameters to meet the desired performance criteria, ensuring robust performance across a range of operating conditions.

Stability Analysis Criteria: The robust stability of the H-infinity controlled system is verified by ensuring that the closed-loop system satisfies the H-infinity norm condition. This condition requires that the maximum singular value of the closed-loop transfer function is less than one for all frequencies, indicating that the system can attenuate disturbances within the specified bounds. Additionally, the stability is confirmed by checking that the poles of the closed-loop system lie in the left half of the complex plane. This ensures that the system will not exhibit unstable behavior or unbounded responses. By meeting these criteria, the H-infinity controller guarantees that the system remains stable and performs robustly even in the presence of uncertainties and disturbances.

Implementation Considerations: The practical implementation of the H-infinity controller involves

integrating it with the sensor system using robust control software tools. These tools, such as MATLAB's Robust Control Toolbox, facilitate the design and implementation of H-infinity controllers by providing functions for model formulation, optimization, and analysis. The designed controller is then programmed into the control system, ensuring compatibility with the existing hardware setup, including the Double Link (DL) sensor and actuators. The integration process involves configuring the con- troller to receive real-time feedback from the sensors, compute the optimal control actions, and send signals to the actuators. This setup ensures that the H-infinity controller can operate effectively in real-time, providing robust vibration isolation and maintaining system stability across a wide range of conditions.

V. RESULTS AND DISCUSSIONS

The aforementioned controllers have been integrated into the system, and their performance has been thoroughly analyzed. The simulation heavily relies on MATLAB/Simulink environment. A comprehensive comparison of the controllers' efficiency within the proposed system has been conducted. These findings are intended to provide a foundational framework for future researchers and real-time implementation endeavors.

The Fig. 4 illustrates the frequency response of the system under the influence of a PID controller. Notably, the sensor utilized is immune to tilt horizontal coupling, as demonstrated in reference (2), with a detailed explanation provided in [1]. Consequently, the focus of this depiction is solely on the control of translation motion, with the tilt response being negligible. When a PID controller is implemented to control a system, the frequency response curve shifts up compared to the one without the controller due to the enhancements in the system's dynamics introduced by the PID control. Specifically, the PID controller adds proportional, integral, and derivative actions that modify the system's transfer function, introducing additional poles and zeros. These modifications typically lead to an increase in the overall system gain, especially at lower frequencies where the integral action dominates, effectively improving the system's ability to track setpoints and reject disturbances. The proportional and derivative actions further refine the system's response by adjusting the overall gain and improving the phase margin, respectively. This combination of increased gain and enhanced stability characteristics results in an upward shift of the frequency response curve. Despite the satisfactory response achieved by the PID controller, the alternative variants—P, PI, and PD—tend to deliver acceptable outcomes only when their respective parameters (Kp, Ki, and Kd) are set to very large values. This phenomenon stems from the inherent limitations of these controllers in addressing specific control aspects. While a PID controller provides a balanced combination of proportional, integral, and derivative actions, the individual variants may struggle to adequately address specific aspects of the system's behavior. For instance, a Proportional (P) controller might fail in overcoming inertia or time delays, necessitating excessively high proportional gains (Kp) for satisfactory performance. Integral (I) control, aimed at eliminating steady-state errors, can lead to integral windup if not carefully managed, especially in the presence of disturbances or uncertainties. Meanwhile, Derivative (D) control, intended to dampen overshoot and improve transient response, can amplify noise and exhibit sensitivity to sudden changes, potentially requiring large derivative gains (Kd) to be effective.

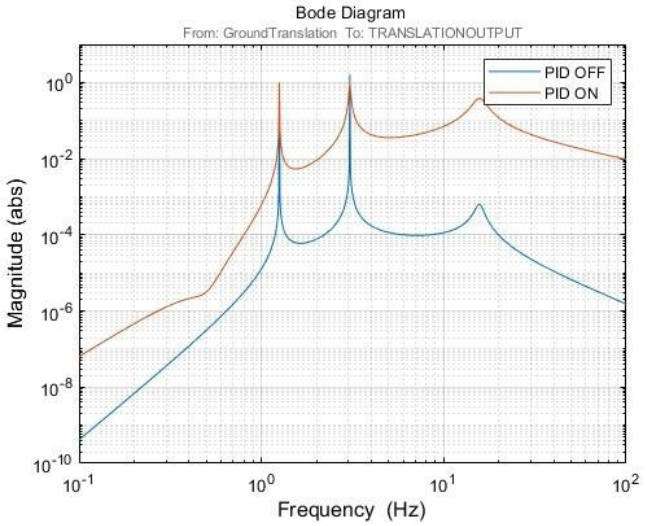

Fig. 4. The frequency response of the system to translation with PID controller off (blue line) and on (red line)

The Fig. 5 illustrates the frequency response of the system under the influence of a LQR controller. As explained earlier, the focus of this depiction is solely on the control of translation motion, with the tilt response being negligible. Observing the graph, it's evident that the LQR controller plays a crucial role in dampening low-frequency vibrations within the system. LQR optimization seeks to minimize a cost function that combines both control effort and system performance. By appropriately tuning the weighting matrices, Q and R, the controller can still be tailored to prioritize certain aspects of control, such as minimizing error or minimizing control effort, based on the system's requirements. Here the response is similar to PID but can be further improved by Q and R tuning.

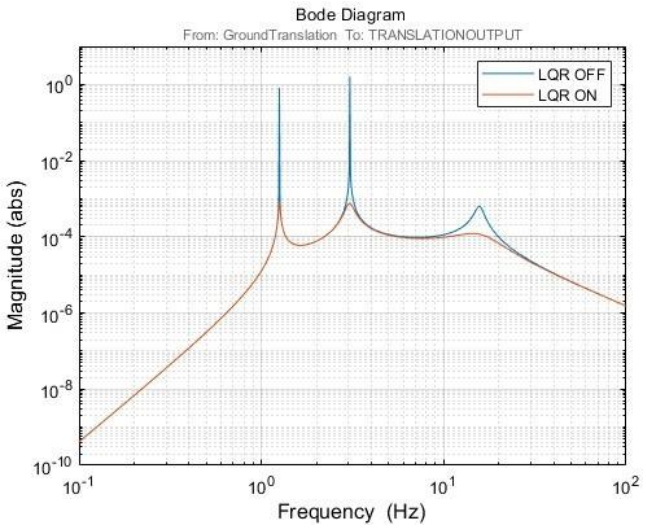

Fig. 5. The frequency response of the system to translation with LQR controller off (blue line) and on (red line)

The plot depicted in Fig. 6 showcases the frequency response of the system when influenced by an LQG controller. Upon examination, it becomes apparent that the response closely resembles that of the LQR case. However, the primary disparity lies in their operational mechanisms: while LQR relies on states as inputs, LQG computes inputs using Kalman filtering. Despite this contrast, both controllers exhibit comparable performance within the system under consideration.

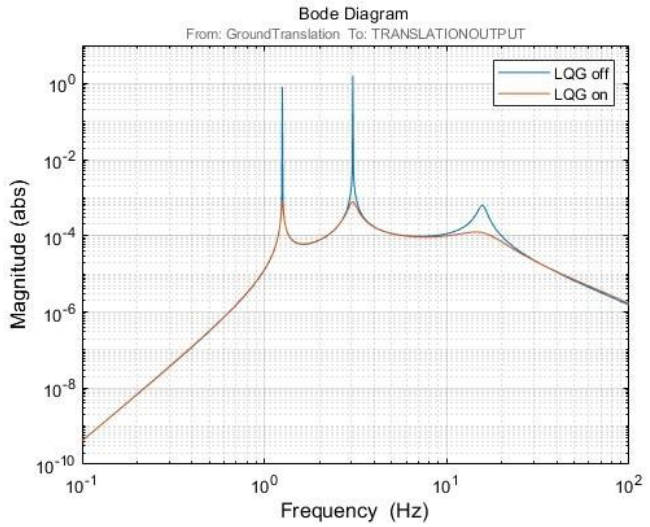

Fig. 6. The frequency response of the system to translation with LQG controller off (blue line) and on (red line)

Selecting the Q and R matrices for LQR (Linear Quadratic Regulator) and LQG (Linear Quadratic Gaussian) controllers is a crucial step in designing effective control systems for complex dynamic systems. These matrices play a pivotal role in defining the control objectives, balancing trade-offs between performance metrics, and ensuring robustness against disturbances and uncertainties.

In the context of LQR, the Q matrix determines the relative importance of each state variable in the cost function that the controller aims to minimize. Typically, Q is a diagonal matrix where each diagonal element represents the weighting assigned to a specific state variable, such as position, velocity, or other relevant state parameters. Higher values in Q indicate that minimizing deviations in those states is more critical for achieving desired system performance. The R matrix in LQR specifies the weighting on control effort or input, influencing how aggressively the controller acts to achieve the desired state trajectories defined by Q. A higher value of R penalizes larger control inputs, promoting smoother control actions and potentially reducing overshoot or oscillatory behavior. Balancing Q and R is crucial: increasing Q weights enhances tracking performance for specific states but may amplify noise sensitivity or require more aggressive control inputs to achieve desired responses. Conversely, adjusting R affects control effort and stability margins, with larger R values potentially increasing control authority but also sensitivity to measurement noise and disturbances.

For LQG controllers, the selection of Q and R matrices integrates state estimation through a Kalman filter, adding complexity and flexibility in handling both control and estimation errors. The Q matrix in LQG is similar to LQR, defining the relative importance of state deviations in the cost function. However, in LQG, Q also influences the Kalman filter's estimation process by weighting the importance of deviations between predicted and actual states. This dual role of Q ensures that control decisions account for both measurement noise and model uncertainties, improving overall system robustness and performance. The R matrix in LQG controls the relative importance of control effort, similarly to LQR, but also interacts with the Kalman filter's covariance matrices to balance trade- offs between control performance and state estimation accuracy. Tuning Q and R matrices in LQG involves iterative adjustments based on system dynamics, noise characteristics, and desired control objectives. Optimizing Q balances tracking accuracy and robustness against disturbances, while R influences control action smoothness and response speed. In practice, selecting Q and R matrices requires a deep understanding of system dynamics, noise characteristics, and operational requirements. Experimental validation and simulation studies are essential to iteratively refine these matrices, ensuring that the control system achieves desired performance metrics such as settling time, overshoot, and robustness to disturbances. Moreover, sensitivity analysis evaluates the impact of parameter variations on stability margins and robustness, guiding the final parameter selection process.

The plot depicted in Fig. 7 showcases the frequency response of the system when influenced by an H-infinity controller. It is evident that the system response is shifted to low frequency side, which makes it a good candidate for the proposed system control. The shift of the frequency response towards the low-frequency side when employing an H-infinity controller can be due to several effects. These controllers are engineered for robust stability in the face of uncertainties, often introducing additional dynamics, especially at lower frequencies, to prevent instabilities. Additionally, inherent dynamics of the controller, such as significant gain or phase lag at lower frequencies, play a role in shaping the closed-loop system response, contributing to the observed shift.

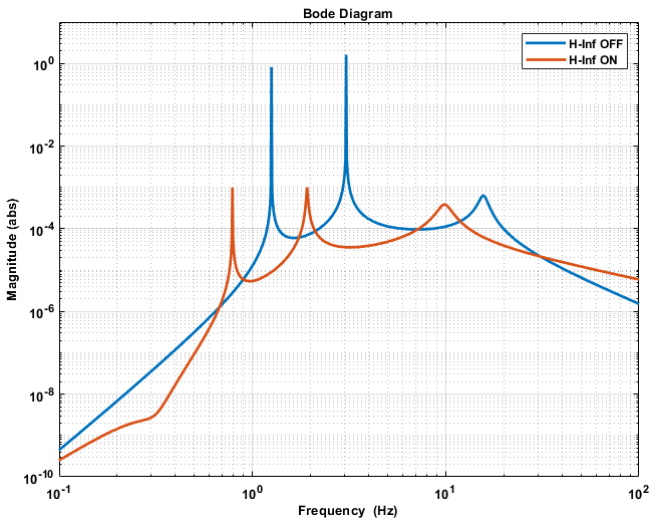

Fig. 7. The frequency response of the system to translation with H-inf controller off (blue line) and on (red line)

A. *Robustness Analysis*

The PID controller, while straightforward and effective in many applications, has inherent limitations in robustness. It relies on fixed parameters (proportional gain Kp, integral gain Ki, derivative gain Kd) that are tuned based on system characteristics. In practical scenarios, disturbances and uncertainties can affect the system's dynamics, potentially leading to sub- optimal performance or instability if the gains are not appropriately adjusted. The integral action, for instance, can lead to integral windup in the presence of significant disturbances, causing overshoot or prolonged settling times. Robustness in PID controllers is typically addressed through careful tuning and sometimes by implementing anti-windup mechanisms to mitigate integral windup effects. The LQR controller is de- signed to optimize system performance based on a quadratic cost function that balances control effort and performance. It provides robustness by inherently minimizing the effects of disturbances and uncertainties that are included in the system model's dynamics matrix A. However, LQR's robustness is tied to the accuracy of the system model; inaccuracies can lead to sub-optimal control performance. Robust stability is often analyzed through the eigenvalues of the closed-loop system matrix, ensuring that all poles lie within the left half of the complex plane. Sensitivity analysis of the weighting matrices Q and R can also provide insights into the controller's robustness against variations in performance requirements. The LQG controller extends the LQR framework by incorporating state estimation through a Kalman filter, which improves robustness against disturbances and uncertainties that affect the measurement process. The Kalman filter estimates the state variables using both the system model and measurement data, reducing the impact of noise and inaccuracies in sensor measurements. Robust stability in LQG controllers is evaluated through the separation principle, ensuring that the controller and estimator operate independently yet effectively together. This principle enhances the controller's robustness by separating the estimation and control tasks, thereby maintaining stability even in the presence of model uncertainties and measurement noise. The H-infinity controller is specifically designed to handle uncertainties and disturbances robustly across a wide range of operating conditions. It achieves this robustness by minimizing the worst-case gain from disturbances to the error signal, thereby ensuring stability and performance under uncertain environments. Robust stability analysis in H-infinity control involves verifying that the closed-loop system satisfies the H-infinity norm condition, which bounds the sensitivity of the system to uncertainties. The controller's design typically involves shaping the controller dynamics to attenuate disturbances effectively without amplifying noise or introducing instability at critical frequencies. Implementation considerations often include trade-offs between robustness and performance, as increased robustness may sometimes come at the expense of control effort or dynamic response speed.

In summary, each controller—PID, LQR, LQG, and H-infinity—offers varying degrees of robustness against disturbances and uncertainties, with trade-offs in complexity, performance, and implementation requirements. Evaluating robust- ness involves considering theoretical stability criteria alongside practical implications such as sensor noise, environmental variability, and hardware constraints, ensuring reliable performance in real-world applications like seismic isolation and gravitational wave detection.

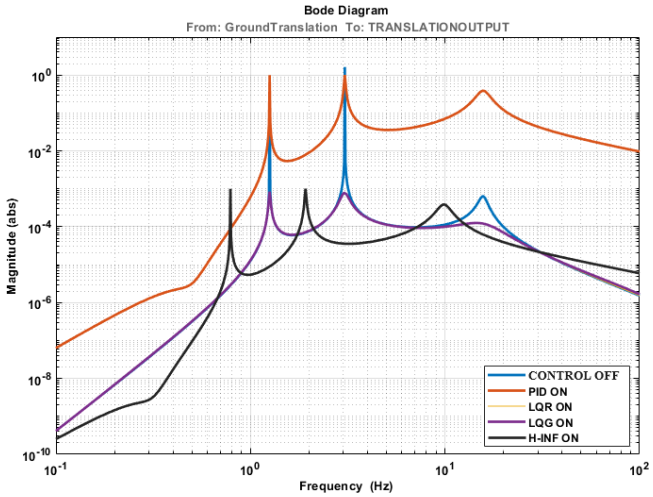

Fig. 8. The frequency response of the translation system to all proposed controllers. H-infinity controller is giving promising result

B. *Comparison of Controller Performance*

The plot in Fig. 8 compares the performance of various controllers in the proposed system. All controllers perform well at low frequencies, but the PID controller exhibits an additional gain. The LQR and LQG controllers are the most promising, delivering satisfactory performance compared to the other two. The LQR controller, while effective, requires state extraction from the system, which can be challenging in practical applications. Conversely, the LQG controller does not have this requirement, making it a more practical choice. But the H-infinity controller shifts the response to even lower frequencies, which is beneficial for our goal of low-frequency vibration isolation. Thus, the H- infinity controller emerges as an excellent candidate for implementing active vibration isolation systems with double pendulum sensors.

Our primary focus in this study was on frequency response analysis for low-frequency applications such as seismic isolation and gravitational wave detection. The controllers we analyzed—PID, LQR, LQG, and H-infinity—were chosen for their unique strengths in managing low-frequency vibrations and mitigating tilt horizontal coupling. Each controller's performance was compared within the context of the sensor system presented in this paper (please refer to Fig. 8), which highlights the performance differences among the controllers in mitigating tilt horizontal coupling. Our aim is to study the feasibility of using the DL sensor for active low-frequency vibration isolation applications. The efficiency of the DL sensor compared to other existing methodologies is already clearly stated in reference [1].

VI. CONCLUSION

In conclusion, this research addresses the significant challenge of horizontal tilt coupling in inertial sensors, particularly in applications such as seismology and gravitational wave detection. By implementing the Double Link (DL) sensor in an active vibration isolation setup and

employing various control algorithms including PID, LQR, LQG, and H-infinity, this study demonstrates promising solutions for precise equipment control. The PID controller effectively dampens low-frequency vibrations, albeit with potential parameter tuning challenges, while the LQR and LQG controllers optimize control effort and yield comparable performance. Notably, the H-infinity controller shows promise in providing robust stability against uncertainties, despite the observed shift in the frequency response towards lower frequencies. These findings contribute valuable insights into the trade-offs and strengths of each controller type, informing future developments in the field. Overall, this research represents a significant step towards enhancing the effectiveness and precision of inertial sensor applications in critical fields like gravitational wave detection, with implications for the advancement of scientific endeavors such as the Einstein Telescope project.

In addition to gravitational wave detection and seismology, our study suggests several promising areas where the controllers could be effectively applied. For instance, healthcare robotics presents an opportunity to enhance precision and stability in robotic surgery systems using advanced controllers like LQR and LQG. Similarly, in environmental monitoring, PID controllers could play a pivotal role in sensor networks for maintaining accurate positioning in air quality monitoring stations. Additionally, integrating H-infinity controllers into smart grids could bolster stability and resilience against disturbances, thereby contributing to the reliability of modern power distribution systems. To address current limitations and optimize practical implementation, future research efforts could focus on improving sensor integration techniques to mitigate noise and enhance robustness in variable environmental conditions. Moreover, optimizing computational efficiency of controller algorithms for real-time processing on embedded systems would ensure scalability and applicability to larger-scale systems. Empirical validation remains crucial for validating the effectiveness of our findings in real-world scenarios. Therefore, future studies should prioritize experimental setups to corroborate simulation results and identify any discrepancies, thereby refining con- troller designs for enhanced practical performance.

ACKNOWLEDGEMENT

The authors would like to thank Manipal Institute of Technology, MAHE Manipal for providing the facilities required for this research.

REFERENCES

[1] V. G. Nair and C. Collette, “Double link sensor for mitigating tilt-horizontal coupling,” *Journal of Instrumentation*, vol. 17, 2022, doi: 10.1088/1748-0221/17/04/ P04012.

[2] N. V. Bondada, A., “Dynamics of multiple pendulum system under a translating and tilting pivot.,” *Arch Appl Mech*, vol. 93, 2023, doi: 10.1007/s00419-023-02473-6.

[3] F. Matichard and M. Evans, “Review: Tilt-free low-noise seismometry,” *Bull. Seismol. Soc. Am.*, vol. 105, 2015, doi: 10.1785/0120140200.

[4] C. Collette *et al*., “Review: Inertial sensors for low frequency seismic vibration measurement,” *Bull.Seismol. Soc. Am.*, vol. 102, 2012, doi: 10.1785/0120110223.

[5] F. Matichard *et al*., “Modeling and experiment of the suspended seismometer concept for attenuating the contribution oftilt motion in horizontal measurements,” *Rev. Sci. Instrum.*, vol. 87, 2016, doi: 10.1063/1.4953110.

[6] N. Rijnveld, R. van den Braber, P. R. Fraanje, and T. C. van den Dool, “Low- frequency vibration isolation in six degrees of freedom: The hummingbird,” in *Proceedings of the euspen International Conference– Delft- June 2010*, 2010, doi:10.1109/IMCCC.2015.75.

[7] W. Hua. *Low frequency vibration isolation and align- ment system for advanced ligo*. Ph.D. Thesis, Stanford University, Stanford, U.S.A, 2005.

[8] C. Mow-Lowry and D. Martynov, “A 6d interferometric inertial isolation system,” *Class. Quant. Grav*, vol. 36, 2019, doi: 10.1088/1361-6382/ab4e01.

[9] C. Speake and D. Newell, “The design and application of anovel high-frequency tiltmeter,” *Rev. Sci. Instrum*, vol. 61, 1990, doi: 10.1063/1.1141160.

[10] J. Winterflood, Z. B. Zhou, L. Ju, and D. G. Blair, D. G, “Tilt suppression for ultra-low residual motion vibration isolation in gravitational wave detection,” *Phys. Lett A*, vol. 277, 2000, doi: 10.1016/S0375-9601(00)00689-7.

[11] Y. Cheng, J. Winterflood, L. Ju, and D. Blair, “Tilt sensor and servo control system for gravitational wave detection,” *Class. Quant. Grav.*, vol. 19, 2002, doi: 10.1088/ 0264-9381/19/7/367.

[12] A. Sunderland *et al*., “High performance rotational vibration isolator,” *Rev. Sci. Instrum.*, vol. 84, no. 10, 2013, doi: 10.1063/1. 4825342.

[13] F. Matichard *et al*., “Modeling and experiment of the suspended seismometer concept for attenuating the contribution of tiltmotion in horizontal measurements,” *Rev. Sci. Instrum.*, vol. 87, 2016, doi: 10.1063/1.4953110.

[14] A. Marrocchesi, “A prototype for a tilt-free seismometer, ligoconsortium, technical note,” *LIGO-T1500485v1 2015/10/17*, vol. 87, 2015.

[15] L.-H. Wu, Y. Huang, R.-Y. Qi, Z. Lv, and B. Sun, “Anew low-frequency active vibration isolation system,” in *2015 Fifth International Conference on Instrumentation and Measurement, Computer, Communication and Control(IMCCC)*, pp. 322–325, 2015. doi:10.1109/IMCCC.2015. 75.

[16] L. Chen *et al*., “Theoretical and experimental study on vibration sensitivity of cubic cavity for space applications,” *Optics Laser Technology*, vol. 158, p. 108915, 2023, doi: 10.1016/j.optlastec.2022.108915.

[17] M. U. Demir and C. Yilmaz, “Analysis and design of an adjustable stiffness three-axis horizontal vibration isolator using elastic columns and a string in tension,” *Journalof Sound and Vibration*, vol. 523, p. 116736, 2022, doi: 10.1016/j.jsv.2021.116736.

[18] L. Liu *et al*., “Modeling and suppression of atomic co- magnetometer’s response to micro-vibration,” *Sensors andActuators A: Physical*, vol. 359, p. 114503, 2023, doi: 10.1016/j.sna.2023.114503.

[19] B. Ding, G. Zhao, J. Watchi, A. Sider, and C. Collette, “An interferometric inertial sensor for low-frequency seismic isolation,” *Sensors and Actuators A: Physical*, vol. 335, p. 113398, 2022, doi: 10.1016/j.sna.2022.113398.

[20] J. Chen, L. Wang, J. Lin, and Y. Tang, “A pendulum actuatorfor environmental vibration isolation based on magnetostrictive composite material,” *Sensors and Actuators Reports*, vol. 4, p. 100134, 2022, doi: 10.1016/j.snr.2022. 100134.

[21] A. S. Ubhi, J. Bryant, D. Hoyland, and D. Martynov, “Cryogenic optical shadow sensors for gravitational wave detectors,” *Cryogenics*, vol. 126, p. 103547, 2022, doi: 10.1016/j. cryogenics.2022.103547.

[22] J. Winterflood, Z. B. Zhou, L. Ju, and D. G. Blair, “Tilt suppression for ultra-low residual motion vibration isolation in gravitational wave detection,” *Physics Letters A*, vol. 277,no. 3, pp. 143–155, 2000, doi: 10.1016/S0375-9601(00)00689-7.

[23] S. K. Sharma, R. C. Sharma, and J. Lee, “Modelling and simulation of mr damper characterization and uncertainty assessment in marine engine vibration isolation with flpid control,” *International Journal of Modelling and Simulation*, pp. 1-11, 2024, doi: 10.1080/02286203.2024.2327465.

[24] D. Luo, Y. Su, B. Zhang, H. Peng and X. Zhou, "Design and simulation of active ultra-low frequency vertical vibration isolator for atom interferometry," *2020 Chinese Automation Congress (CAC)*, pp. 7640-7643, 2020, doi: 10.1109/CAC51589.2020.9327348.

[25] Z. Zhang, Z. Yuan and X. Li, "A New Active Negative Stiffness Control Strategy for Improving Low-Frequency Vibration Isolation Performance," *2023 3rd International Conference on Electrical Engineering and Control Science (IC2ECS)*, pp. 801-805, 2023, doi: 10.1109/IC2ECS60824.2023. 10493674.

[26] T. Huynh, D. -H. Lee, and Y. -B. Kim, "A Study on Robust Noninteracting Control System Design with Disturbance Feedforward for 6-DoF Active Vibration Isolation Platform," *2022 International Symposium on Semiconductor Manufacturing (ISSM)*, pp. 1-6, 2022, doi: 10.1109/ISSM55802.2022.10026944.

[27] W. Shi, K. Liu, and W. Zhao, "Active Vibration Isolation of a Maglev Inertially Stabilized Platform Based on an Improved Linear Extended State Observer," in *IEEE Access*, vol. 9, pp. 743-751, 2021, doi: 10.1109/ACCESS.2020.3046886.

[28] S. Zhang *et al*., "Adjustable indentation and vibration isolation performances of nacre-like metamaterial," *International Journal of Smart and Nano Materials*, vol. 14, no. 3, pp. 303-320, 2023. doi: 10. 1080/19475411.2023.2221668.

[29] D. Li, F. Liu, J. Deng, Z. Tang, and Y. Wang, "Nonlinear Damping Curve Control of Semi-Active Suspension Based on Improved Particle Swarm Optimization," in *IEEE Access*, vol. 10, pp. 90958-90970, 2022, doi: 10.1109/ACCESS.2022.3201867.

[30] X. Liang and J. Yuan, "An absolute-zero-stiffness vibration isolator for continuously varying mass: theoretical design and numerical simulation," *Mechanics of Advanced Materials and Structures*, vol. 31, no. 20, pp. 5075-5089, 2024, doi: 10.1080/15376494. 2023.2211408.

[31] W. Gong, A. Li, J. Ma, P. Wu, and F. Qin, "An Ultralow-Frequency Vertical Isolation System Based on Composite Feedforward and Feedback Control," in *IEEE Sensors Journal*, vol. 23, no. 23, pp. 29109-29118, 2023, doi: 10.1109/JSEN.2023. 3321920.

[32] S. Wen, J. Jing, D. Cui, Z. Wu, W. Liu, and F. Li, "Vibration isolation of a double-layered Stewart platform with local oscillators," *Mechanics of Advanced Materials and Structures*, vol. 29, no. 27, pp. 6685-6693, 2023, doi: 10.1080/15376494.2021. 1983896.

[33] X. Yang *et al*., "Dynamics and Isotropic Control of Parallel Mechanisms for Vibration Isolation," in *IEEE/ASME Transactions on Mechatronics*, vol. 25, no. 4, pp. 2027-2034, 2020, doi: 10.1109/TMECH.2020.2996641.

[34] H. Zhang, W. Xiao, and F. Zhang, "Dynamic analysis and experimental investigation of particle damping for the vibration reduction and isolation of floating raft using the two-phase flow theory of gas-particle," *Ships and Offshore Structures*, pp. 1-15, 2024, doi: 10.1080/17445302.2024.2312731.

[35] Z. Zhu *et al*., "A Compliant Self-Stabilization Nano positioning Device with Modified Active–Passive Hybrid Vibration Isolation Strategy," in *IEEE/ASME Transactions on Mechatronics*, vol. 28, no. 6, pp. 3305-3316, 2023, doi: 10.1109/TMECH.2023.3265329.

[36] J. Tang, Y. Yang, C. Dou, Y. Li, and D. Cao, "Micro-vibration control of spaceborne payload with smart parallel struts," *Mechanics of Advanced Materials and Structures*, pp. 1-15, 2024, doi: 10.1080/15376494.2024.2329798.

[37] B. Yan, X. Wang, H. Ma, W. Lu, and Q. Li, "Hybrid Time-Delayed Feedforward and Feedback Control of Lever-Type Quasi-Zero-Stiffness Vibration Isolators," in *IEEE Transactions on Industrial Electronics*, vol. 71, no. 3, pp. 2810-2819, 2024, doi: 10.1109/TIE.2023.3269481.

[38] J. Yao, K. Wu, M. Guo, G. Wang, and L. Wang, "An Ultralow-Frequency Active Vertical Vibration Isolator With Geometric Antispring Structure for Absolute Gravimetry," in *IEEE Transactions on Instrumentation and Measurement*, vol. 69, no. 6, pp. 2670-2677, 2020, doi: 10.1109/TIM.2019. 2927545.

[39] J. Liu, X. Zhang, C. Wang, and R. Yan, "Active Vibration Control Technology in China," in *IEEE Instrumentation & Measurement Magazine*, vol. 25, no. 2, pp. 36-44, April 2022, doi: 10.1109/ MIM.2022.9756383.

[40] S. Yang and M. Jia, "Numerical analysis for isolation of vibrations by pile rows in transversely isotropic saturated media due to moving loads," *Mechanics of Advanced Materials and Structures*, pp. 1-18, 2023, doi: 10.1080/15376494. 2023.2215761.

[41] J. Ding *et al*., "The Design of a Sub-Hz Magnetic-Suspended Geophone," in *IEEE/ASME Transactions on Mechatronics*, vol. 27, no. 6, pp. 5824-5834, 2022, doi: 10.1109/ TMECH.2022.3189406.

[42] L. Y. Lu, G. L. Lin, K. W. Pong, and C. L. Liu, "Experimental verification and performance evaluation of an inertia-type bidirectional isolation system," *Mechanics Based Design of Structures and Machines*, vol. 52, no. 7, pp. 4503-4526, 2024, doi: 10.1080/15397734.2023.2229420.

[43] X. Xie, P. He, D. Wu, and Z. Zhang, "Ultra-low frequency active vibration isolation in high precision equipment with electromagnetic suspension: Analysis and experiment," *Precision Engineering*, vol. 84, pp. 91-101, 2023, doi: 10.1016/ j.precisioneng.2023.07.004.

[44] H. Song, X. Shan, W. Hou, C. Wang, K. Sun, and T. Xie, "A novel piezoelectric-based active-passive vibration isolator for low-frequency vibration system and experimental analysis of vibration isolation performance," *Energy*, vol. 278, p. 127870, 2023, doi: 10.1016/j.energy.2023.127870.

[45] K. Yu, Y. Chen, C. Yu, P. Li, Z. Ren, J. Zhang, and X. Lu, "Origami-inspire quasi-zero stiffness structure for flexible low-frequency vibration isolation," *International Journal of Mechanical Sciences*, vol. 276, p. 109377, 2024, doi: 10.1016/j.ijmecsci. 2024.109377.

[46] L. Zhang, S. Zhang, J. Gao, J. Yi, H. Wen, Y. Chen, and X. Chen, "Design and implementation of a precision levelling composite stage with active passive vibration isolation," *Robotics and Computer–Integrated Manufacturing*, vol. 89, p. 102744, 2024. doi: 10.1016/j.rcim.2024.102744.

[47] H. Pu *et al*., "An active geophone based on a magnetic spring design for low-frequency vibration measurement," *Mechanical Systems and Signal Processing*, vol. 217, p. 111521, 2024, doi: 10.1016/j.ymssp.2024.111521.

[48] T. You, J. Zhou, D. J. Thompson, D. Gong, J. Chen, and Y. Sun, "Vibration reduction of a high-speed train floor using multiple dynamic vibration absorbers," *Vehicle System Dynamics*, vol. 60, no. 9, pp. 2919-2940, 2022, doi: 10.1080/00423114.2021.1928248.

[49] A. Xu, Z. Xu, H. Zhang, S. He, and L. Wang, "Novel coarse and fine stage parallel vibration isolation pointing platform for space optics payload," *Mechanical Systems and Signal Processing*, vol. 213, p. 111359, 2024, doi: 10.1016/j.ymssp.2024. 111359.

[50] A. Xu, Z. Xu, H. Zhang, L. Wang, and S. He, "An adaptive feed-forward active vibration isolation algorithm for input disturbance unbalanced MIMO systems," *Signal Processing*, vol. 217, p. 109346, 2024, doi: 10.1016/j.sigpro.2023.109346.

[51] P. Ling, L. Miao, B. Ye, J. You, W. Zhang, and B. Yan, "Ultra-low frequency vibration isolation of a novel click-beetle-inspired structure with large quasi-zero stiffness region," *Journal of Sound and Vibration*, vol. 558, p. 117756, 2023, doi: 10.1016/j.jsv. 2023.117756.

[52] X. Liu, K. Zhang, H. Shi, F. Hong, H. Liu, and Z. Deng, "Origami-inspired metamaterial with compression–twist coupling effect for low-frequency vibration isolation," *Mechanical Systems and Signal Processing*, vol. 208, p. 111076, 2024, doi: 10.1016/j.ymssp.2023.111076.

[53] R. Zhang, Y. Yang, C. Ma, J. Jiang, X. Liu, H. Yue, and Y. Lu, "A novel low-stiffness blade gear for micro-vibration isolation: Design, modeling, and verification," *Mechanical Systems and Signal Processing*, vol. 211, p. 111223, 2024, doi: 10.1016/j.ymssp.2024.111223.

[54] C. Liu, W. Zhang, K. Yu, T. Liu, and Y. Zheng, "Quasi-zero-stiffness vibration isolation: designs, improvements and applications," *Engineering Structures*, vol. 301, p. 117282, 2024, doi: 10.1016/ j.engstruct.2023.117282.

[55] A. Wang, S. Wang, H. Xia, G. Ma, L. Zhang, and W. Liu, "Adaptive neural control of microgravity active vibra- tion isolation system subject to output constraint and unexpected disturbance," *Acta Astronautica*, vol. 213, pp. 168-176, 2023, doi: 10.1016/j.actaastro.2023.08.040.

[56] H. Ma, K. Wang, H. Zhao, C. Zhao, J. Xue, C. Liang, and B. Yan, "Harnessing chiral buckling structure to design tunable local resonance metamaterial for low-frequency vibration isolation," *Journal of Sound and Vibration*, vol. 565, p. 117905, 2023, doi: 10.1016/j.jsv.2023.117905.

[57] B. Zhao, W. Shi, B. Wang, and J. Tan, "An adjustable anti-resonance frequency controller for a dual-stage actuation semi-active vibration isolation system," *Frontiers of Information Technology & Electronic Engineering*, vol. 22, no. 10, pp. 1390-1401, 2022, doi: 10.1631/FITEE.2000373.

[58] Y. Liu, X. Wang, Y. Xue, E. Deng, Y. Wang, C. Song, and Q. Feng, "Dynamic analysis of quasi-zero stiffness vibration isolation system coupled with frequency adjustable dynamic vibration absorber," *Archive of Applied Mechanics*, vol. 92, no. 12, pp. 3631-3647, 2022, doi: 10.1007/s00419-022-02253-8.

[59] Z. Chai, X. Song, J. Zang, and Y. Zhang, "Nonlinear vibra- tion isolation of spacecraft system by a bionic variable- stiffness device enhanced by electromagnetic component," *Acta Mechanica Solida Sinica*, vol. 36, no. 6, pp. 921-932, 2023, doi: 10.1007/ s10338-023-00431-x.

[60] G. Jin, Z. Wang, and T. Yang, "Cascaded quasi- zero stiffness nonlinear low-frequency vibration isolator inspired by human spine," *Appl. Math. Mech.*, vol. 43, no. 6, pp. 813-824, 2022, doi: 10.1007/s10483-022-2852-5.

[61] B. Yan, N. Yu, and C. Wu, "A state-of-the-art review on low-frequency nonlinear vibration isolation with electromagnetic mechanisms," *Applied Mathematics and Mechanics*, vol. 43, no. 7, pp. 1045-1062, 2022, doi: 10.1007/s10483-022-2868-5.

[62] S. Zhou, D. Zhang, B. Hou, and Z. Ren, "Vibra- tion isolation performance analysis of a bilateral supported bio-inspired anti-vibration control system," *Appl. Math. Mech.*, vol. 44, no. 5, pp. 759-772, 2023, doi: 10.1007/s10483-023-2988-6.

[63] G. Sui *et al*., "A bio-inspired spider-like structure isolator for low-frequency vibration," *Applied Mathematics and Mechanics*, vol. 44, no. 8, pp. 1263-1286, 2023, doi: 10.1007/s10483-023-3020-9.

[64] K. Xu, M. Niu, Y. Zhang, and L. Chen, "An active high-static-low-dynamic-stiffness vibration isolator with adjustable buckling beams: theory and experiment," *Applied Mathematics and Mechanics*, vol. 45, no. 3, pp. 425-440, 2024, doi: 10.1007/s10483-024-3087-6.

[65] Z. Meng and M. Qiang, "Analysis of vibration isolation effect of double-layer WIB based on wave impedance ratio," *Geotechnical and Geological Engineering*, vol. 41, no. 6, pp. 3699-3714, 2023, doi: 10.1007/ s10706-023-02482-w.

[66] Y. Chai and X. Jing, "Low-frequency multi-direction vibration isolation via a new arrangement of the X-shaped linkage mechanism," *Nonlinear Dynamics*, vol. 109, no. 4, pp. 2383-2421, 2022, doi: 10.1007/ s11071-022-07452-0.

[67] X. Song, Z. Chai, Y. Zhang, J. Zang, and K. Xu, "Nonlinear vibration isolation via an innovative active bionic variable stiffness adapter (ABVSA)," *Nonlinear Dynamics*, vol. 109, no. 2, pp. 353-370, 2022, doi: 10.1007/ s11071-022-07495-3.

[68] Y. Yu, F. Li, and G. Yao, "Vibration response and isolation of X-shaped two-stage vibration isolators: Analysis of multiple parameters," *Nonlinear Dynamics*, vol. 111, no. 17, pp. 15891-15910, 2023, doi: 10.1007/s11071-023-08704-3.

[69] H. Ou, X. Sun, Q. Wu, Z. Chen, Z. Chen, Q. Chen, and L. Hu, "A novel bio-inspired kangaroo leg structure for low-frequency vibration isolation," *Nonlinear Dynamics*, vol. 112, no. 3, pp. 1797-1814, 2024, doi: 10.1007/s11071-023-09082-6.

[70] S. Zhou, B. Hou, L. Zheng, P. Xu, T. Yu, and Z. Ren, "Nonlinear property and dynamic stability analysis of a novel bio-inspired vibration isolation–absorption structure," *Nonlinear Dyn.*, vol. 112, no. 2, pp. 887-902, 2024, doi: 10.1007/s11071-023-09084-4.

[71] K. Yu, Y. Chen, C. Yu, J. Zhang, and X. Lu, "A compact nonlinear stiffness-modulated structure for low-frequency vibration isolation under heavy loads," *Nonlinear Dynamics*, vol. 112, no. 8, pp. 5863-5893, 2024, doi: 10.1007/s11071-024-09334-z.

[72] T. Yang, Y. Zhang, and S. Zhou, "Multistage oscillators for ultra-low frequency vibration isolation and energy harvesting," *Science China Technological Sciences*, vol. 65, no. 3, pp. 631-645, 2022, doi: 10.1007/s11431-021-1952-1.

[73] X. Zhang, X. Liu, C. Sun, Q. Pan, and T. He, "Improvement of vibration isolation performance of multi-mode control seat suspension system through road recognition using wavelet-LSTM approach," *Journal of Mechanical Science and Technology*, vol. 38, no. 1, pp. 121-136, 2024, doi: 10.1007/ s12206-023-1210-2.

[74] C. Wei, "Low-frequency vibration isolation via new wide range zero-stiffness isolator with multiple negative stiff- ness mechanisms," *Journal of the Brazilian Society of Mechanical Sciences and Engineering*, vol. 46, no. 3, p. 120, 2024, doi: 10. 1007/s40430-024-04710-7.

[75] B. Wang, Z. Jiang, and P. D. Hu, "Study on 6-DOF active vibration-isolation system of the ultra-precision turning lathe based on GA-BP-PID control for dynamic loads," *Advances in Manufacturing*, vol. 12, no. 1, pp. 33-60, 2024, doi: 10.1007/s40436-023-00463-z.

[76] C. Wei, "Design and analysis of a novel vehicle-mounted active qzs vibration isolator," *Iranian Journal of Science and Technology, Transactions of Mechanical Engineering*, vol. 47, no. 4, pp. 2121-2131, 2024, doi: 10.1007/s40997-023-00622-4.

[77] W. Liu *et al*., "Flight test results for microgravity active vibration isolation system on-board Chinese Space Station," *npj Microgravity*, vol. 10, no. 1, p. 19, 2024, doi: 10.1038/s41526-024-00359-7.

[78] X. Yin, Y. Xu, X. Sheng, S. Wan, and Y. Wang, "Study on the Micro-vibration Suppression of a MnCu Spring Isolation Platform with Low Stiffness and High Damping," *International Journal of Aeronautical and Space Sciences*, vol. 24, no. 3, pp. 753-765, 2023, doi: 10.1007/s42405-02.

[79] X. Xing, Z. Chen, and Z. Feng, "A variable stiffness and damping control strategy for improving vibration isolation performances in low-frequency excitation," *Journal of Vibration Engineering & Technologies*, vol. 11, no. 4, pp. 1595-1608, 2023, doi: 10.1007/s42417-022-00659-w.

[80] J. Hu *et al*., "Research on an Active Vibration Isolation System with Hybrid Control Strategy for The Guidance System of TBM," *Journal of Vibration Engineering & Technologies*, vol. 12, no. 1, pp. 773-782, 2024, doi: 10.1007/s42417-023-00874-z.

[81] S. Wang, L. Yu, Q. Zhang, and R. Xiang, "Design and Analysis of a Novel Horizontal Large-Amplitude and Low-Frequency Vibration Isolator," *Journal of Vibration Engineering & Technologies*, vol. 12, no. 4, pp. 6155-6167, 2024, doi: 10.1007/ s42417-023-01244-5.

[82] G. F. Franklin, J. D. Powell, A. Emami-Naeini, and J. D. Powell. *Feedback control of dynamic systems* (vol. 4). Upper Saddle River: Prentice Hall, 2002.

[83] D. E. Kirk. *Optimal control theory: an introduction*. Courier Corporation, 2004.

[84] J. P. Hespanha. *Linear Systems Theory: Second Edition*. Princeton University Press, 2018.

[85] J. C. D. Kemin Zhou and K. Glover. *Robust and Optimal Control*. Pearson, 1995.